

# Optimal communication frequency for switching cabled ocean networks with commands carried over the power line<sup>\*</sup>

Yan-hu CHEN<sup>†‡</sup>, Yu-jia ZANG, Jia-jie YAO, Gul MUHAMMAD

State Key Laboratory of Fluid Power and Mechatronics Systems, Zhejiang University, Hangzhou 310027, China

<sup>†</sup>E-mail: yanhuchen@zju.edu.cn

Received Mar. 4, 2019; Revision accepted Aug. 12, 2019; Crosschecked Oct. 10, 2019

**Abstract:** Cabled ocean networks with tree or ring topologies play an important role in real-time ocean exploration. Due to the time-consuming need for field maintenance, cable switching technology that can actively switch the power on/off on certain branches of the network becomes essential for enhancing the reliability and availability of the network. In this paper, a novel switching-control method is proposed, in which we invert the power transmission polarity and use the current on the power line as the digital signal at low frequency to broadcast information with the address and commands to the network, and the corresponding branching unit (BU) can decode and execute the switching commands. The cable's parasitic parameters, the network scale, and the number of BUs, as the influencing factors of the communication frequency on the power line, are theoretically studied and simulated. An optimized frequency that balances the executing accuracy and rate is calculated and proved on a simulated prototype. The results showed that the cable switching technology with optimized frequency can enhance the switching accuracy and configuring rate.

**Key words:** Cable switching; Cabled ocean network; Branching unit; Transmission line theory; Communication frequency  
<https://doi.org/10.1631/FITEE.1900125>

**CLC number:** TP271

## 1 Introduction

Seventy percent of the Earth's surface is covered by ocean and this plays a decisive role in climate change, ocean ecosystems, and evolution and development of living species. However, human beings have historically known very little about the ocean due to the paucity of ways to explore it until the past few decades, when real-time in situ observation systems (especially cabled ocean networks) were initiated and constructed. Cabled ocean networks, commonly composed of tens of backbone nodes, hundreds of removable sub-nodes, and thousands of scientific instruments covering thousands of square kilometers on the seafloor, can provide abundant power and

broad bandwidth communication for undersea experiments. These experiments enable the study of ocean processes on or below the seafloor, in the water column and on the sea surface, over wide time and spatial scales (Aguzzi et al., 2011).

Large-scale cabled multi-node ocean networks with tree or ring topologies, covering hundreds or thousands of square kilometers, have been gradually adopted for long-term and real-time ocean observation and are recognized as a permanent part of the seafloor infrastructure. In addition, compared with a mesh topology, ocean networks with tree or ring topologies have the advantages of low construction costs and easy maintenance. Thus, they are easy to apply in engineering practice, whether they run constant current (CC) or constant voltage (CV) (Hsu et al., 2007; Hsiao et al., 2014; Zhang et al., 2015; Hishiki et al., 2016). The observatory is composed mainly of a shore station (SS), a submarine optic-electric cable with a single conductor, branching units (BUs), and

<sup>‡</sup> Corresponding author

<sup>\*</sup> Project supported by the National Natural Science Foundation of China (No. 51409229)

 ORCID: Yan-hu CHEN, <http://orcid.org/0000-0002-5020-7355>

© Zhejiang University and Springer-Verlag GmbH Germany, part of Springer Nature 2019

science nodes. In the tree topology (Fig. 1a), monopolar negative high-voltage power (normally  $-10$  kV) is delivered via the single conductor of the cable with seawater as the return path to reduce electrode electrolytic corrosion, power loss, and costs. Therefore, each node and SS have an individual electrode for current flow. The science nodes are connected to the spur cables branching from the backbone cable through the BUs. High-voltage power is reduced to a conventional level and distributed to the connected terminal instruments in the observation nodes (Chen et al., 2013). The cable switching method physically switches power on/off to certain nodes at the BUs remotely controlled from the SS, to properly locate/isolate a fault, make field maintenance without shutdown of nominal parts, or run upgrades with minimum interference to the running system. Thus, it would be highly advantageous if cable switching could be involved, through which each branch could be actively switched on or off.

For a large-scale underwater network, power and communication transmission are the two main functions that can be realized via a single optic-electric submarine cable. Usually, the copper conductor of the submarine cable is used for power delivery, while the optical fibers are used for communication. Unfortunately, ground faults and short faults are the major faults that can occur, and they can easily induce communication failure, even power collapse. For an ocean network powered by CC, such as DONET (Kawaguchi et al., 2008) and DONET2 (Kawaguchi et al., 2013), as shown in Fig. 1b, when an unexpected state occurs in the nodes, the BUs and repeater on the backbone cable can still work normally because of the CC power supply. At this time, BUs can be remotely controlled by the SS to bypass the fault node. Similarly, in NEPTUNE (Schneider and Liu, 2005; Barnes et al., 2013), although the main science nodes are powered by CV, the repeaters and BUs are powered by the current in the cable, and the current can be converted to CV to power the internal equipment. When ground faults and short faults occur, although the main science nodes may not work properly, once there is sufficient current in the cable (at this time, the power supply may be forced to enter the CC output mode), the repeaters and BUs can still work properly and communicate directly with the SS via the optical fiber. Hence, a systematic topology reconfiguration

can be carried out to isolate the fault nodes as much as possible.

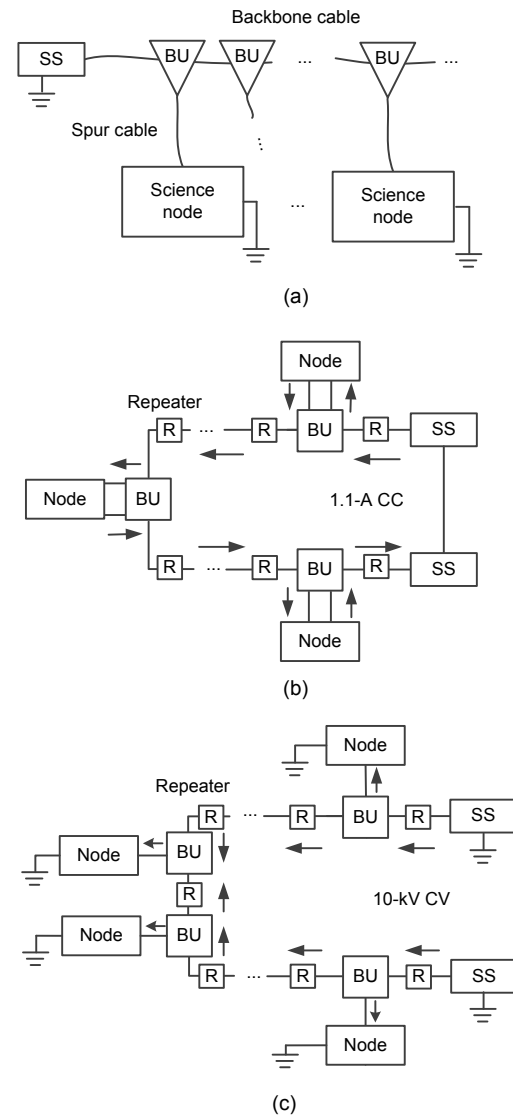


**Fig. 1 Typical architectures of the cabled ocean network: (a) cabled ocean network with tree topology; (b) equivalent power architecture diagram of DONET2; (c) equivalent power architecture diagram of NEPTUNE Canada** Each node may have different sub-nodes connected, which are not shown in the figure

However, the above methods are relatively complex and expensive, and additional optical fibers are required for large-scale ocean networks. Once the optical fiber breaks, the corresponding nodes will lose the ability to communicate with the SS. Therefore, transferring information through the conductor to reconfigure the system is an alternative solution. As the candidate solution for the NEPTUNE Canada, a

method was proposed that simply changes the voltage level and polarity as commands to control the interrupters of each BU (El-Sharkawi et al., 2005; Lu and Shuai, 2006). However, all actions operated based on local hardware detection are totally autonomous, so the system has no ability to actively control specific interrupters to switch on or off (Qu et al., 2015). Chen et al. (2015) developed an actively controllable switching and offline operation method, which is based on discrete current as the command signal and features zero current and nearly zero voltage switching. The advantage of the CV power system includes high power transmission efficiency, extension flexibility, and power capacity when it is used for power delivery, and the advantages of the CC mode include fault tolerance to a short fault when it is used for network configuration/cable switching. However, the proposed method operates a network with a very limited number of nodes (less than 10) because the value of the discrete current cannot be too low and is not suitable for a large system. To solve the problem of the limited number of nodes and possible unreliability due to the discrete current used, a method of broadcasting addresses and commands using digital voltage signals was introduced (Zhang et al., 2018). Nonetheless, once ground faults and short faults occur on the backbone cables, there is some difficulty in maintaining the voltage signal. However, with the current being used as the digital signal to broadcast commands, even if ground faults and short faults occur on the backbone cable, the commands can still be normally broadcasted, which will be studied in detail in this study.

Hence, based on the previously mentioned work focusing on the tree topology, in this study, a CV cabled ocean observatory (Fig. 1) is adopted to discuss the corresponding switching system. Also, by adopting the hybrid CC-CV system from Chen et al. (2015), which can work in the CV mode in a normal scenario and work in the CC mode during a maintenance scenario, we propose a new cable switching method that works by inverting the power transmission polarity and varying the current on the power line with low frequency to broadcast information including addresses and commands to the network, where the BU with the right address can execute the switching commands. Therefore, more BUs and interrupters can be controlled with high reliability.

## 2 Switching system design

### 2.1 Underlying concepts of the switching system

The CC-CV hybrid system is designed to share the same power conductor and requires no extra cables or communication devices. CC and CV are applied in two modes separately, maintenance mode and normal operating mode.

#### 1. Maintenance mode

Unlike previous traditional fault isolation and isolation methods (Schneider and Liu, 2005; Chan et al., 2007), in this study, coded current through the conductor in the cables is designed as the digital signal to transmit addresses and commands to each BU, which requires the CC output mode of the power source in the SS. The control logic of the switching method is shown in Fig. 2. The current sensing resistor and the voltage comparator convert the current digital signal into the standard transistor-transistor logic (TTL) digital signal. After it is decoded by the microcontroller unit (MCU), a specific switching action can be executed. This coded current should be able to supply the electrical energy required by the BUs. Furthermore, all the maintenance control is carried out with the nodes on the spur cables not working. Therefore, the interrupters are operated only under zero current and voltage, maximizing their lifetime and improving the reliability of the network. In this mode, the operator can roughly locate short faults (if presented) by switching off each branch and section one by one and using the voltammetry algorithm or another method to calculate the location. Similarly, the operator can reconfigure the network, such as isolating fault sections/nodes or repairing/upgrading parts in the field.

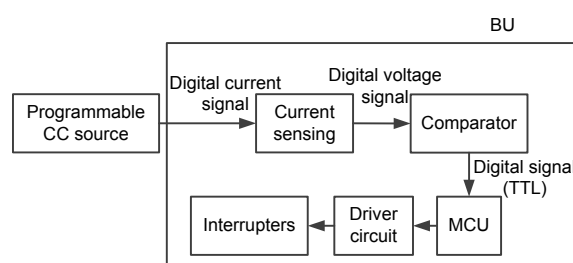


Fig. 2 Control logic of the BU in the maintenance mode

#### 2. Normal operating mode

In this mode, the SS feeds the network with negative high voltage (normally around  $-10$  kV)

power and works in the CV mode. The high voltage goes through the interrupters to power the nodes on the spur cables. The BU controller should be blocked to avoid malfunction of the interrupters.

## 2.2 Switching system structure

As shown in Fig. 3, the special electrical structural requirements that make the aforementioned concept possible are as follows:

1. Two latch-type vacuum interrupters ( $S_1$  and  $S_2$ ) route to the backbone cable and spur cable accompanying a serial high-voltage diode ( $D_2$  and  $D_3$ ) for selection of the current direction. Each interrupter has two companion solenoids that are electrically isolated, one for closing and one for opening.

2. The switching system circuit consists of a switch for two closing solenoids ( $S1\_C$  and  $S2\_C$ ), two opening solenoids ( $S1\_O$  and  $S2\_O$ ), a current-sensing resistor ( $R_{sam}$ ) for sampling the varying current signal, a Zener diode (ZD) tapping a stable voltage to energize the switch controller and the switch driving circuit, and a high-voltage diode ( $D_1$ ) for current direction selection.

3. An additional individual cathode terminates at the end of the cable for CC current return.

Based on these features, the aforementioned two modes can be achieved:

1. Maintenance mode. With the positive current,  $D_2$  and  $D_3$  make the coded CC flow through the BU controllers and block the entering interrupters or nodes; i.e., all current in the backbone cable flows through the current-sensing resistor  $R_{sam}$ . At this time, the MCU is powered by the voltage drop of the ZD.

2. Normal operating mode. With the negative voltage, due to the diode  $D_1$ , there is not enough current to supply MCU, ensuring that  $S_1$  and  $S_2$  will not act in this mode.

## 2.3 Switching system communication protocol

The programmable power source in the SS is controlled by the computer and it can output the specific current waveform. When the MCU decodes the command signals with the same communication protocol, it can issue a signal to drive the corresponding interrupter through the drive circuit. This shows that the premise of precise digital control of an underwater switch is to develop a unified communication protocol.

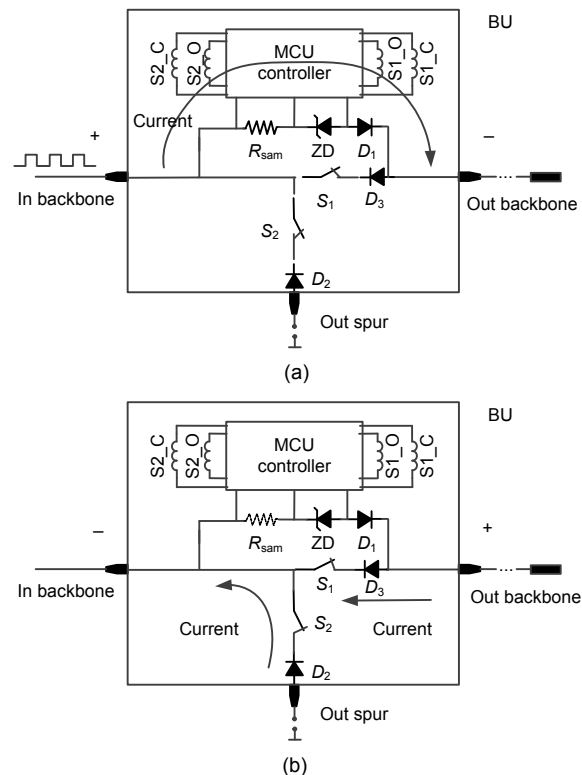


Fig. 3 Switching circuit of the BU under the maintenance scenario (a) and normal scenario (b)

Fig. 4 shows the communication protocol of the switching system. Only when the MCU samples a falling edge will the switch controller be activated. The data package is composed of the following five parts: start bit, address bits, command bits, parity bit, and stop bit. The address bits include address information, which is the license to control a specific switching system. Each switching system has a unique address ID. When the number of science nodes increases, we need to increase only the number of address bits. In theory, the number of controllable nodes can reach  $2^n$  with  $n$  address bits. The command bits control the final status of the two interrupters of each BU. The parity bit is used to confirm whether the data format is correct. The stop bit is a flag bit used to tell the switch controller that the command signals are over.

When the data flowing on the transmission lines meets the data format of the established communication protocol, the corresponding interrupter in the specific BU will take actions. Any data frame error will lead to failure of the entire control command or even switch malfunction. Therefore, whether the

controller can correctly sample the digital current signals is the key to the overall control process of the switching system. However, the main factor that affects the system identification is noise, which comes mainly from the power source, transmission path, and electronic components. The digital current signals are transmitted to the switching systems from the SS through the existing power transmission path, usually with hundreds or even thousands of kilometers of cable. Here, the noise affecting the signal integrity is considered mainly to be from the transmission cable with different parasitic capacitances, inductances, and parasitic resistances (Meng et al., 2004; Righini et al., 2018). The parasitic capacitances, inductances, and parasitic resistances distort digital current signals to varying degrees, and the distortion can even cause the encoding information to be misinterpreted from the original code of 0 to the code of 1. Such a decoding error can directly lead to the failure of switch control. In the following sections, we study mainly the power transmission lines and the dynamic response of the output current waveform during the entire transmission process.

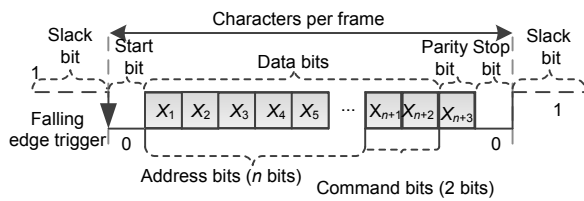


Fig. 4 Communication protocol definition

### 3 Switching system modeling

Generally, the parasitic parameters of the optic-electric submarine cable are along the direction of the transmission line distribution and are evenly distributed. The cable model can be considered a single uniform lossy transmission line (single-core wire supply, in which the other loop is seawater, assuming that seawater is a good conductor whose relevant parasitic parameters are zero) (Song and Breitholtz, 2016). To facilitate the study of voltage and current on the transmission lines with time and space transformation, the binary functions  $u(x, t)$  and  $i(x, t)$  are used in this study. The resistance, inductance, capacitance, and conductance of the unit length cable are  $R_0$  ( $\Omega/\text{km}$ ),  $L_0$  ( $\text{H}/\text{km}$ ),  $C_0$  ( $\text{F}/\text{km}$ ), and  $G_0$  ( $\text{S}/\text{km}$ ),

respectively. For example, one of the cables used in ocean networks is a coaxial optic-electric cable with an added double-layer armored structure, with the specific parameters of  $R_0=1 \Omega/\text{km}$ ,  $L_0=0.37 \text{ mH}/\text{km}$ , and  $C_0=0.16 \mu\text{F}/\text{km}$ , which are provided by the supplier.

The real distributed parameter model is shown in Fig. 5. According to the Kirchhoff voltage and current law, we can obtain

$$\begin{cases} u(x, t) - \left( u(x, t) + \frac{\partial u(x, t)}{\partial x} dx \right) \\ = R_0 dx \cdot i(x, t) + L_0 dx \cdot \frac{\partial i(x, t)}{\partial t}, \\ i(x, t) - \left( i(x, t) + \frac{\partial i(x, t)}{\partial x} dx \right) \\ = G_0 dx \cdot \left( u(x, t) + \frac{\partial u(x, t)}{\partial x} dx \right) \\ + C_0 dx \cdot \frac{\partial}{\partial t} \left( u(x, t) + \frac{\partial u(x, t)}{\partial x} dx \right). \end{cases} \quad (1)$$

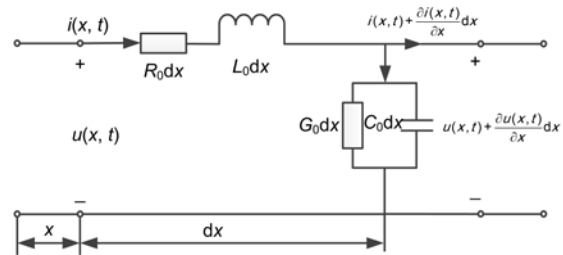


Fig. 5 Distributed parameter cable model

Omitting the second-order items and carrying out the Laplace transform in Eq. (1), we have

$$\begin{cases} -\frac{dU(x, s)}{dx} = (R_0 + sL_0)I(x, s), \\ -\frac{dI(x, s)}{dx} = (G_0 + sC_0)U(x, s). \end{cases} \quad (2)$$

Hence, the general solution of Eq. (2) is

$$\begin{cases} U(x, s) = A_1(s)e^{-\gamma(s)x} + A_2(s)e^{\gamma(s)x}, \\ I(x, s) = Z_c^{-1}(s)[A_1(s)e^{-\gamma(s)x} - A_2(s)e^{\gamma(s)x}], \end{cases} \quad (3)$$

where  $\gamma(s) = [(R_0 + sL_0)/(G_0 + sC_0)]^{1/2}$  and  $Z_c(s) = [(R_0 + sL_0)/(G_0 + sC_0)]^{1/2}$  are the characteristic impedance and transmission coefficient, respectively (Sun et al., 2011).

The general system power supply and the voltage source related in the theoretical research are used for this method; however, it is the current source discussed in this study. Eq. (3) is only a theoretical derivation result for the distributed parameter cable model. The boundary condition is not added to Eq. (3), and  $A_1(s)$  and  $A_2(s)$  are still unknown. Combined with the specific BU shown in Fig. 3, we make appropriate and reasonable simplification for the cable switching system as follows: We theorize that the actual current source is equivalent to a large resistance and the ideal current source in parallel. The total cable length is  $l$ . As the sampling resistance is excessively small compared with the cable's parasitic resistance, and the voltages across the ZD and diode are constant, the switching system can be simplified to be shorted. The exclusive electrode of the BU control system is directly connected to the seawater to form a complete circuit; therefore, the equivalent circuit on the load side is also shorted. The simplified equivalent system model is shown in Fig. 6.

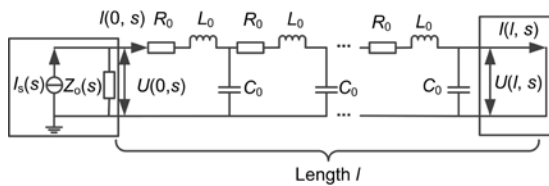


Fig. 6 Equivalent model of the switching system

For Eq. (3), let  $x=0$ . Then we have

$$\begin{cases} U(0, s) = A_1(s) + A_2(s), \\ I(0, s) = Z_c^{-1}(s)[A_1(s) - A_2(s)]. \end{cases} \quad (4)$$

At the side of the current source, with the Kirchhoff current law applied, we can obtain

$$I(0, s) = I_s(s) - \frac{U(0, s)}{Z_o(s)} = I_s(s) - \frac{A_1(s) + A_2(s)}{Z_o(s)}. \quad (5)$$

Since the load side of the equivalent circuit is shorted, the terminal voltage must be zero. Therefore, with Eq. (3), we can obtain

$$U(l, s) = A_1(s)e^{-\gamma(s)l} + A_2(s)e^{\gamma(s)l} = 0. \quad (6)$$

Combining Eqs. (4)–(6), we have

$$\begin{cases} A_1(s) = \frac{-e^{2\gamma(s)l} I_s(s) Z_o(s) Z_c(s)}{(1 - e^{2\gamma(s)l}) Z_c(s) - (1 + e^{2\gamma(s)l}) Z_o(s)}, \\ A_2(s) = \frac{I_s(s) Z_o(s) Z_c(s)}{(1 - e^{2\gamma(s)l}) Z_c(s) - (1 + e^{2\gamma(s)l}) Z_o(s)}. \end{cases} \quad (7)$$

For simplification, we make

$$\begin{aligned} m(s) &= \frac{Z_o(s)}{(1 - e^{2\gamma(s)l}) Z_c(s) - (1 + e^{2\gamma(s)l}) Z_o(s)} \\ &= \frac{1}{(1 - e^{2\gamma(s)l}) \frac{Z_c(s)}{Z_o(s)} - (1 + e^{2\gamma(s)l})}. \end{aligned} \quad (8)$$

For the ideal current source,  $Z_o(s)$  is infinite. Hence, we obtain

$$m(s) \approx -1/(1 + e^{2\gamma(s)l}). \quad (9)$$

Ultimately, we can obtain the current value at any position and any time in the  $s$  domain throughout the transmission cable combining Eqs. (3), (7), and (9):

$$I(x, s) = \frac{e^{2\gamma(s)l} e^{-\gamma(s)x} + e^{\gamma(s)x}}{1 + e^{2\gamma(s)l}} I_s(s). \quad (10)$$

The common analytical inversion method is to use the line integral method to achieve the inverse transformation, and then we need to calculate the residue of product expression at each pole. However, in the actual engineering problem, the Laplace space solution is often quite complex or has multiple poles, and the differential operation is difficult to achieve by hand. In this study, the Stehfest algorithm as shown in Eq. (11) is adopted for its simple structure, not involving complex arithmetic. It can be simply programmed as

$$\begin{cases} f(t) = \frac{\ln 2}{t} \sum_{i=1}^N V_i F(s_i), \\ V_i = (-1)^{\frac{N}{2}+i} \cdot \sum_{k=\frac{i+1}{2}}^{\min(i, \frac{N}{2})} \frac{k^{\frac{N}{2}} (2k)!}{\left(\frac{N}{2} - k\right)! k!(k-1)!(2k-i)!}, \\ s_i = \frac{\ln 2}{t} \cdot i, \end{cases} \quad (11)$$

where  $N$  is even and under normal circumstances, and  $N$  takes 16. This algorithm simplifies the complex  $s$  domain polynomial  $F(s)$  into  $f(t)$  by means of a discrete summation method (Sheng et al., 2011). For the switching system, given input source  $I_s(s)$  and Eq. (10), we can easily convert  $I(s, t)$  to  $i(x, t)$  by a numerical solution, which is of great significance for the study of the optimal communication rate in the power line.

The distributed parameter cable model can accurately describe the parameters and the distribution status of the actual transmission line; however, the TLOSSY model, which is a uniformly distributed parameter cable model in the software PSPICE (sub-product of Cadence Design Systems Inc.), cannot converge when inputting a step signal. Moreover, we cannot build an actual cable model in the lab due to the distribution parameters in the micro-segment  $dx$ . Therefore, we have used a cascade-lumped parameter model where the transmission line unit is a certain length of the cable. In a finite length of the cable, we use the lumped parameter  $\pi$ -type to simulate a section of the cable, and the ground conductivity  $G_0$  is ignored here (Ma et al., 2009; Araújo et al., 2014). The specific cascade-lumped parameter  $\pi$ -type cable model is shown in Fig. 7, where  $R_0$ ,  $L_0$ , and  $C_0$  are the parasitic resistance, inductance, and capacitance per unit length, respectively, and  $n$  is the equivalent length of the per-lumped parameter model. Hence, the equivalent resistance and inductance of the finite length cable are  $R_0n$  and  $L_0n$ , respectively. The equivalent capacitance  $C_0n$  is evenly distributed on both sides of the equivalent inductance and resistance.

Now, we can use software simulation and the above system's mathematical model to determine a reasonable cascade accuracy, namely, the length of the cascade cable  $n$ , making the cable equivalent model error for the switching system within an acceptable range. On one hand, we use the PSPICE software to simulate the output current value of the terminal with different cascade precision  $n$  (5, 10, 20, 50, and 100 km). On the other hand, according to the above theoretical deduction with the distribution parameter cable model, the result  $i(x, t)$  with the Stehfest numerical inversion will be compared with the above simulation results. Both methods use the unit step input source, and the main inspection is the time increase of the current at the end. Here, we select the

600 km total cable length to elaborate the results (Table 1). It can be seen that the better the cable cascade accuracy, the more it can represent the distributed parameter cable model. Limited by the laboratory space and production, we choose 10-km cascade accuracy for the cable, and the results of the simulation and theoretical calculation with the distributed parameter cable model are close. The relative error of the rise time is  $\delta=(50.8-50.1)/50.1 \times 100\%=1.4\%$ , which is small enough to prove the accuracy of the transfer function formula and the correctness of choosing the 10-km cascade accuracy. Therefore, in the next process for software simulation and model construction of the transmission lines in the laboratory, the 10-km cascade precision will be used to simulate the actual transmission lines.

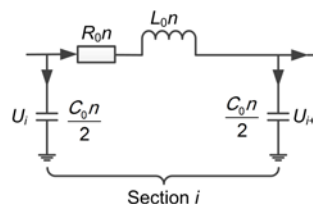


Fig. 7 Cascade-lumped parameter  $\pi$ -type cable model

Table 1 Rise time under unit step current

Number of the $\pi$ -type models	Cascade precision (km)	Rise time (ms)
Infinite*	Infinitesimal*	50.8
120	5	50.3
60	10	50.1
30	20	49.0
12	50	46.3
6	100	42.1

\* Distributed parameters calculated by Eqs. (10) and (11). Other results are obtained by simulation from PSPICE

#### 4 Optimal communication frequency

As the channel of the entire digital control system is the existing power line, the line with different length has different attenuation and delay effects for the high-frequency components in the digital current signal. When the total cable length increases, the time that one bit lasts will also increase (that is to say, the digital communication rate drops), so that the switching system can accurately sample the digital signals. Hence, the optimal communication frequency of the digital current signals should be determined to

ensure that each BU controller can accurately detect the input signals. The digital communication should be as fast as possible. Furthermore, the switching control commands are a series of current square wave signals with high and low current values, and the change in the two current values can be taken as a step transition (Fig. 8).

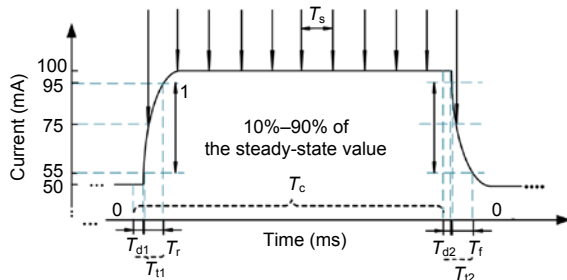


Fig. 8 Distorted square current wave

We define the time interval where the curve transmits from the steady-state value of 10% to 90% and 90% to 10% as the rise time  $T_r$  and fall time  $T_f$ , respectively, and the delay times of the rising edge and falling edge are  $T_{d1}$  and  $T_{d2}$ , respectively. The sum of  $T_r$  and  $T_{d1}$  is equal to the transition time  $T_{t1}$ , the sum of  $T_f$  and  $T_{d2}$  is equal to the transition time  $T_{t2}$ , the transmission time is  $T_c$  (the corresponding communication frequency  $f_c$ ), and the sampling time is  $T_s$  (the corresponding sampling frequency  $f_s$ ). The simulation results and theoretical analysis show that the transition times of the rising edge and the falling edge are basically the same. Here, only the transient characteristics ( $T_{d1}$ ,  $T_r$ , and  $T_{t1}$ ) of the rising edge of the signal are considered.

For large ocean networks, the cable's parasitic parameters are large. If the magnitude of the current in the transmission lines is large, the voltage drop on the lines caused by parasitic resistance may exceed the cable transmission capacity range and break down the cable insulation directly. However, the current level cannot be too small; otherwise, it cannot provide the switch drive circuit of the BU with enough energy to complete the established switch task. At the same time, we find that the average current value and the peak-to-peak current value of the digital current signals will not affect the transient characteristics. Considering the scale of the submarine system, voltage tolerance of the transmission lines, decoding identification, and the energy demand of the BU circuits,

we select a digital signal of 0=50 mA and a digital signal of 1=100 mA.

The model of the switching system is built in the simulation. The cable length of the switching system is 600 km with a total of three BUs, and each BU has a space of 200 km. Complete BU modules have been added into the system software simulation process. The simulation system uses a 10-km cascade accuracy of a  $\pi$ -type cable model. The cable-related parasitic parameters are the same as those described in the previous section. The power supply side is a step current signal from 50 to 100 mA, and we measure the current waveforms of the cable at 0, 200, 400, and 600 km. It can be seen from the simulation results (Fig. 9) that the farther away the SS power supply is, the more serious the output current distortion is, compared with the input current (or the larger the characteristic parameters  $T_r$  and  $T_d$  will become in the time domain). At 600 km, the rise time  $T_r=51.0$  ms, the delay time  $T_d=4.5$  ms, and the transition time  $T_t=T_r+T_d=55.5$  ms are the maxima of this specific switching system. Therefore, the distortion of the control signals is the most serious at the farthest position away from the SS power supply. Thus, we need to measure only the transition time of the current for the farthest location on the transmission lines to determine the overall distortion of the system.

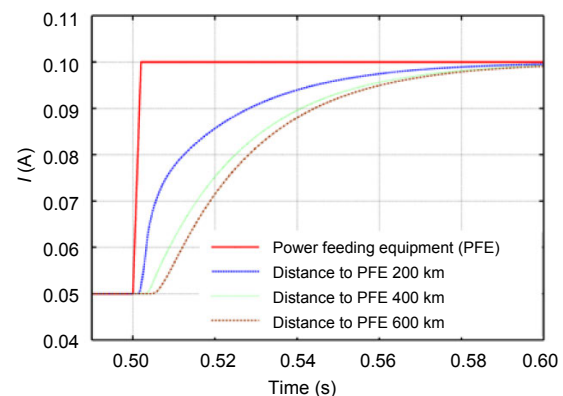


Fig. 9 Time domain responses at different locations on the 600-km cable

A series of simulations for the switching system with various transmission lines from 200 to 2000 km are conducted in the same way. We carry out the measurements of the transient characteristics of  $T_r$ ,  $T_d$ , and  $T_t$  at the end of the transmission lines. The results are shown in Table 2. When the length of the

transmission lines is increasing, the maximum transition time of the whole system is also increasing. The degree of distortion of the input current is intensified. When the length of the transmission cable reaches 2000 km, the transition time of the output current is approximately 597 ms. Such a long transition phase will create a great threat to the sampling accuracy. To make sure that the MCU can accurately sample the digital current signals, MCU sampling time  $T_s$  and transmission time  $T_c$  of each bit current signal increase accordingly.

**Table 2 Simulation results of the transient characteristics**

Length	$T_d$ (ms)	$T_r$ (ms)	$T_t$ (ms)
200	1.0	4.5	5.5
400	2.4	22.1	24.5
600	4.5	51.0	55.5
800	6.3	91.4	97.7
1000	8.0	143.3	151.3
1200	9.5	206.5	216.0
1400	12.6	281.5	294.1
1600	15.1	372.5	387.6
1800	18.1	466.4	484.5
2000	21.6	575.5	597.1

With the existing simulation data and theoretical calculation results, the curve fitting toolbox in Matlab is used to obtain the relationship between the length of transmission lines ( $L$ ) and the maximum transition time ( $T_t$ ). Based on the characteristics of the existing data, we use the common polynomial fitting method to fit the data (Fig. 10). With the second-order polynomial, the relationship between  $T_t$  and  $L$  is obtained within a 95% confidence interval, expressed as

$$T_t = 0.00015L^2 + 0.014L - 4, \quad L < 2000. \quad (12)$$

Furthermore, appropriate sampling methods must be standardized to avoid sampling errors and guarantee correct command recognition (Liao, 2009). Comparing the merits and faults of the sampling methods in terms of an off-the-shelf communication protocol, a 10-time sampling frequency is taken into account:

$$f_s = 10f_c \quad (T_c = 10T_s). \quad (13)$$

Considering the degree of distortion, we simply

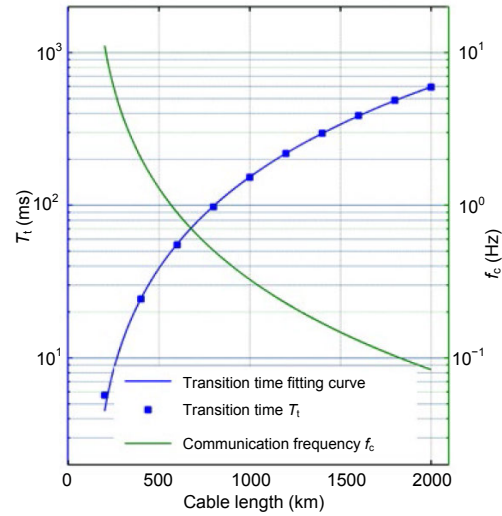


**Fig. 10 Simulated transition time  $T_t$  with its fitting curve**  
The optimal communication frequency of the digital current signals  $f_c$  is obtained by Eq. (14)

consider the influence of the parasitic parameters of the cable. However, for the actual submarine cable, many other uncertain factors will hinder the change in the digital current signals, and some of the disturbances are unavoidable. For example, an electrical vibration or impulse caused by the environment or power source may generate a deviation. Moreover, cable parasitic parameter error, simulation error, curve fitting error, and electronic component response time increase the actual transition time  $T_t$ . To ensure the sampling accuracy, the sampling time  $T_s$  of the switch controller must be larger than  $T_t$ . For example, the rise time of 50 ms gives a nominal sampling frequency of 20 Hz. Set the safety factor  $S=2$ , which reduces the sampling frequency by 50%, that is, 10 Hz. In addition, with a 10-time sampling frequency taken into account, the communication frequency should be one-tenth of its sampling frequency, namely 1 Hz.

For general cases, with the safety factor  $S=2$ , the communication frequency is expressed as

$$f_c = \frac{1000}{T_c} = \frac{1000}{10 \times (2T_t)} = \frac{1000}{20T_t} = \frac{1000}{20(0.00015L^2 + 0.014L - 4)} \quad (14)$$

where  $f_c$  is the optimal communication frequency of the digital current signals (Hz). The dependence of  $f_c$  on length  $L$  is illustrated in Fig. 10.

When transmitting a series of digital current signals over long-distance power lines, the optimal communication rate for digital current signals can be easily determined within 2000 km. This ensures the high integrity of the signals, improves the reliability of the entire control process, and shortens the execution time of the entire control instruction during the long-distance power line transmission process.

## 5 Prototype setup and test

A prototype was built in a laboratory to validate that the proposed CC digital method is feasible and reliable for controlling the switching of the tree topology network (Fig. 11). In the experiments, a test platform composed of 20 RLC circuits was constructed to simulate the 200-km submarine cable. Each RLC mode used a serial 10- $\Omega$  resistance, a serial 3.7-mH inductance, and a parallel 1.6- $\mu$ F capacitance to simulate a 10-km submarine cable. These parameters are consistent with the parasitic parameters above.

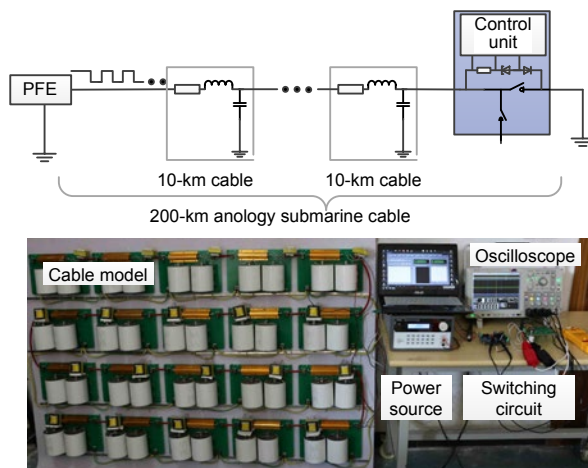


Fig. 11 Experimental setup with a 200-km model cable

The number of branch units does not substantially affect the current waveform, and the waveform parameters of the farthest circuit are the characteristic variables of the whole system; therefore, only one switching system was constructed at the end of the power line. From Eq. (14), the optimal transmission time  $T_c \approx 100$  ms ( $T_s = 5$  ms) leads the frequency of the digital current signals  $f_c$  to be 10 Hz in the switching process. Furthermore, for the latch-type vacuum

interrupter to operate normally, the voltage across the solenoid must be maintained above 16 V for at least 15 ms; therefore, an energy-storage capacitor connected in parallel with each solenoid was configured in each drive circuit, providing the energy to drive the solenoid. Before a response to the command signal was made, enough time was provided for the energy-storage capacitor to store sufficient energy. Both actual measurement and circuit simulation have proven that when the current of the power supply is 100 mA, it takes only approximately 6 s for the storage capacitor voltage to reach 20 V. Therefore, we can increase the length of time for the slack bit (digital bit of 1 when  $i=100$  mA) to meet the requirements of the driving vacuum interrupter.

Set the address bits to be 10101. In addition, two command bits represent the status of the corresponding vacuum interrupter. Bit “1” represents closing the interrupter, whereas bit “0” represents opening the interrupter. Even parity was used, and the stop bit was low level “0.” The experimental results are shown in Fig. 12.

Channel 1 (blue line) represents the input digital current signals flowing through the switching system. Channel 2 (cyan line) represents the voltage across the energy-storage capacitor for driving the opening and closing solenoids. Channels 3 (red line) and 4 (green line) represent the voltages across the closing solenoid and opening solenoid of the interrupter, respectively. Before the switching system can respond to the command, the voltage across the energy-storage capacitor was already at approximately 20 V; thus, the energy was sufficient for driving the solenoids of the interrupters. Fig. 12a shows the command signals to close the interrupter. When the switch controller received a stop bit, the driving signal was sent to the corresponding drive circuit. Energy stored in the capacitor was released to the closing solenoid to close the interrupter, with a decrease in voltage in the capacitor and a voltage pulse across the closing solenoid at the same time. In general, the driving signals from the switch controller would last 80 ms, which was sufficient for the drive circuit to drive the solenoid. Next, the capacitor would restart to store energy for the next command signal. Fig. 12b shows the command signals to open the interrupter. Similar to Fig. 12a, a voltage pulse across the opening solenoid indicated that energy was released to the opening

solenoid to open the interrupter with a decrease in voltage in the energy-storage capacitor. During the entire switch process, no incorrect actions were made by the opposite solenoid and its energy-storage capacitor. Figs. 12c and 12d show the two cases of incorrect command signals. Fig. 12c shows a command signal with an incorrect check bit, and Fig. 12d shows a command signal with non-corresponding address information of 10110. Neither of the two command signals would trigger the operation of the interrupter.

The sampling time was set to twice the rise time, and the cable system drove the sampling frequency at 10 times the digital frequency, which is consistent with the above theoretical deduction. The results showed that we can achieve accurate switching control. When the control switch success rate and reliability are not taken into consideration, the maximum communication rate can reach 250 Hz ( $T_c=4$  ms) in the laboratory test for a 200-km transmission cable. This is almost consistent with the first column results of Table 1. It proves that the cable physical model, mathematical model, and software simulation are correct. Furthermore, a durability test was conducted by transmitting different command signals cyclically and continuously. The opening and closing solenoids were driven 2000 times, and no failure was monitored during the entire test.

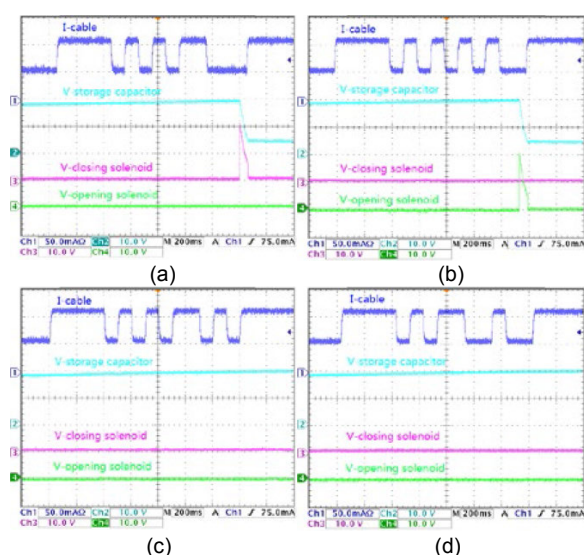


**Fig. 12 Operations with command signals: (a) command to close an interrupter; (b) command to open an interrupter; (c) command with wrong check bit; (d) command with non-corresponding address**

References to color refer to the online version of this figure

## 6 Conclusions and discussion

An active node isolating method based on digital current signals has been introduced for an ocean network. The mathematical model, software simulation, and laboratory model have been established for the fault isolation system. Such a signal integrity analysis has ensured the accuracy and efficiency of the digital control command. However, when the above method is applied in practical engineering, the following aspects must be considered:

1. The switching systems are configured based on the network power transmission path without additional cables or devices. Hence, no communication links exist between the SS and the switching systems, leading to no switching feedback mechanism existing in this method.

2. When the cable is lengthy to a certain degree, each command signal may continue for tens of seconds or even longer. Therefore, the switching method is not suitable for large-scale ocean networks.

3. The optimal communication rate of the current control signals is applicable only to the tree topology, and the star topology or the ring topology is with no multi-level branches. This is because when the topology of the system with multi-level branches is reconfigured by the BUs, the current in the same branch may be different before and after the reconfiguration, and a decoding error is likely to occur.

4. In this study, we do not perform cable parasitic parameter correction for the cable model combined with environmental factors, such as salinity, temperature, and pressure, which may introduce a bias into the digital current signal communication rate, the steady-state analysis, and the fault location.

To summarize, the comparison of the method proposed in this study with several existing methods is shown in Table 3.

### Acknowledgements

The authors would like to thank Zhongtian Technology Submarine Cable Co., Ltd., for suggestions and providing the parameters of the submarine cable.

### Compliance with ethics guidelines

Yan-hu CHEN, Yu-jia ZANG, Jia-jie YAO, and Gul MUHAMMAD declare that they have no conflict of interest.

**Table 3 Comparison of the main characteristics of several switching methods and their application scope**

Method	Advantage	Disadvantage
Optical supervisory method (NEPTUNE, DONET, etc.)	Two-way communication between SS and BUs; capable of remote control; knowable states of BUs	Complicated structure; high cost
El-Sharkawi et al. (2015)'s method	Easy arc extinguishing; automatically isolating the low resistance faults; functional independence of the BUs; low cost	Incapable of remote control; unknown states of BUs
Chen et al. (2015)'s method	Easy arc extinguishing; low cost; capable of remote control	Low control reliability; limited number of BUs; unknown states of BUs; only suitable for the topologies without multiple branches
Zhang et al. (2018)'s method	Easy arc extinguishing; low cost; capable of remote control; unlimited number of BUs	Sensitive to low impedance faults on backbone cables; unknown states of BUs; small communication rate with long cables
Our method	Easy arc extinguishing; low cost; capable of remote control; unlimited number of BUs; relatively high reliability	Unknown states of BUs; Small communication rate with long cables; only suitable for the topologies without multiple branches

## References

- Aguzzi J, Mánuel A, Condal F, et al., 2011. The new seafloor observatory (OBSEA) for remote and long-term coastal ecosystem monitoring. *Sensors*, 11(6):5850-5872. <https://doi.org/10.3390/s110605850>
- Araújo ARJ, Silva RC, Kurokawa S, 2014. Comparing lumped and distributed parameters models in transmission lines during transient conditions. IEEE PES T&D Conf and Exposition, p.1-5. <https://doi.org/10.1109/TDC.2014.6863477>
- Barnes CR, Best MMR, Johnson FR, et al., 2013. Challenges, benefits, and opportunities in installing and operating cabled ocean observatories: perspectives from NEPTUNE Canada. *IEEE J Ocean Eng*, 38(1):144-157. <https://doi.org/10.1109/JOE.2012.2212751>
- Chan T, Liu CC, Howe BM, et al., 2007. Fault location for the NEPTUNE power system. *IEEE Trans Power Syst*, 22(2): 522-531. <https://doi.org/10.1109/TPWRS.2007.894855>
- Chen YH, Yang CJ, Li DJ, et al., 2013. Study on 10 kVDC powered junction box for a cabled ocean observatory system. *China Ocean Eng*, 27(2):265-275. <https://doi.org/10.1007/s13344-013-0023-y>
- Chen YH, Howe BM, Yang CJ, 2015. Actively controllable switching for tree topology seafloor observation networks. *IEEE J Ocean Eng*, 40(4):993-1002. <https://doi.org/10.1109/JOE.2014.2362830>
- El-Sharkawi MA, Upadhye A, Lu S, et al., 2005. North east pacific time-integrated undersea networked experiments (NEPTUNE): cable switching and protection. *IEEE J Ocean Eng*, 30(1):232-240. <https://doi.org/10.1109/JOE.2004.839938>
- Hishiki K, Fujiwara N, Katayama T, et al., 2016. Power distribution system for multidisciplinary seafloor observatory junction box. *Techno-Ocean*, p.325-328. <https://doi.org/10.1109/Techno-Ocean.2016.7890671>
- Hsiao NC, Lin TW, Hsu SK, et al., 2014. Improvement of earthquake locations with the Marine Cable Hosted Observatory (MACHO) offshore NE Taiwan. *Mar Geophys Res*, 35(3):327-336. <https://doi.org/10.1007/s11001-013-9207-3>
- Hsu SK, Lee CS, Shin TC, et al., 2007. Marine Cable Hosted Observatory (MACHO) project in Taiwan. *Int Symp on Underwater Technology and Workshop on Scientific Use of Submarine Cables and Related Technologies*, p.305-307. <https://doi.org/10.1109/UT.2007.370808>
- Kawaguchi K, Kaneda Y, Araki E, 2008. The DONET: a real-time seafloor research infrastructure for the precise earthquake and tsunami monitoring. *MTS/IEEE Kobe Techno-Ocean*, p.1-4. <https://doi.org/10.1109/OCEANSKOB.2008.4530918>
- Kawaguchi K, Araki E, Kogure Y, et al., 2013. Development of DONET2-off Kii channel observatory network. *IEEE Int Underwater Technology Symp*, p.1-5. <https://doi.org/10.1109/UT.2013.6519844>
- Liao Y, 2009. Some algorithms for transmission line parameter estimation. 41<sup>st</sup> Southeastern Symp on System Theory, p.127-132. <https://doi.org/10.1109/SSST.2009.4806781>
- Lu S, Shuai L, 2006. Infrastructure, Operations, and Circuits

- Design of an Undersea Power System. PhD Thesis, University of Washington, Seattle, USA.
- Ma SC, Xu BY, Bo ZQ, et al., 2009. The research on lumped parameter equivalent circuit of transmission line. 8<sup>th</sup> Int Conf on Advances in Power System Control, Operation and Management, p.194.  
<https://doi.org/10.1049/cp.2009.1820>
- Meng H, Chen S, Guan YL, et al., 2004. Modeling of transfer characteristics for the broadband power line communication channel. *IEEE Trans Power Del*, 19(3):1057-1064.  
<https://doi.org/10.1109/TPWRD.2004.824430>
- Qu FZ, Wang ZD, Song H, et al., 2015. A study on a cabled seafloor observatory. *IEEE Intell Syst*, 30(1):66-69.  
<https://doi.org/10.1109/MIS.2015.9>
- Righini D, Passerini F, Tonello AM, 2018. Modeling transmission and radiation effects when exploiting power line networks for communication. *IEEE Trans Electromagn Compat*, 60(1):59-67.  
<https://doi.org/10.1109/TEMC.2017.2728370>
- Schneider K, Liu CC, 2005. Topology error identification for the NEPTUNE power system using an artificial neural network. IEEE PES Power Systems Conf and Exposition, p.94-99. <https://doi.org/10.1109/PSCE.2004.1397439>
- Sheng H, Li Y, Chen YQ, 2011. Application of numerical inverse Laplace transform algorithms in fractional calculus. *J Franklin Inst*, 348(2):315-330.  
<https://doi.org/10.1016/j.jfranklin.2010.11.009>
- Song YJ, Breitholtz C, 2016. Nyquist stability analysis of an AC-grid connected VSC-HVDC system using a distributed parameter DC cable model. *IEEE Trans Power Del*, 31(2):898-907.  
<https://doi.org/10.1109/TPWRD.2015.2501459>
- Sun H, Jin ZJ, Kim MG, et al., 2011. Equivalent-circuit modeling for multilayer capacitors based on coupled transmission-line theory. *IEEE Trans Compon Pack Manuf Technol*, 1(5):731-741.  
<https://doi.org/10.1109/tcpmt.2011.2115241>
- Zhang F, Chen YH, Li DJ, et al., 2015. A double-node star network coastal ocean observatory. *Mar Technol Soc J*, 49(1):59-70. <https://doi.org/10.4031/MTSJ.49.1.7>
- Zhang ZF, Chen YH, Li DJ, et al., 2018. Use of a coded voltage signal for cable switching and fault isolation in cabled seafloor observatories. *Front Inform Technol Electron Eng*, 19(11):1328-1339.  
<https://doi.org/10.1631/FITEE.1601843>